Determination of the antiferromagnetic spin axis in epitaxial $LaFeO_3$ films by x-ray magnetic linear dichroism spectroscopy

J. Lüning,[1] F. Nolting,[1,2,*] A. Scholl,[2] H. Ohldag,[1,2] J. W. Seo,[3,4,†] J. Fompeyrine,[3] J.-P. Locquet,[3] and J. Stöhr[1]
[1]*Stanford Synchrotron Radiation Laboratory, Stanford University, Stanford, California 94309, USA*
[2]*Advanced Light Source, Lawrence Berkeley National Laboratory, Berkeley, California 94720, USA*
[3]*IBM Research Division, Zürich Research Laboratory, 8803 Rüschlikon, Switzerland*
[4]*Institut de Physique, University of Neuchâtel, 2000 Neuchâtel, Switzerland*
(Received 23 August 2002; revised manuscript received 23 December 2002; published 27 June 2003)

We report x-ray magnetic linear dichroism (XMLD) measurements at the Fe $L_{2,3}$ absorption edges of thin antiferromagnetic (AFM) $LaFeO_3$ films grown epitaxially on $SrTiO_3$ (100) and (110) substrates and a stepped (100) substrate with a 2° miscut. The spin structure in the near-surface region of the thin films, and in particular the orientation of the AFM axis, has been derived from the observed polarization dependence. We show that in all cases, the orientation of the AFM axis differs from that of bulk $LaFeO_3$. In particular, we find that the AFM axis is rotated away from its bulk orientation and lies parallel to the (111) plane of the underlying cubic $SrTiO_3$ substrate, with its projection on the film surface parallel to the *c* axis of the orthorhombic $LaFeO_3$ crystal lattice. Our results are of importance in light of existing models for the exchange coupling and bias of antiferromagnetic/ferromagnetic multilayers. They indicate the inadequacy of models that assume a bulk like spin structure near surfaces and interfaces.

DOI: 10.1103/PhysRevB.67.214433 PACS number(s): 75.70.Ak, 75.25.+z, 61.10.Ht

I. INTRODUCTION

Thin film magnetic multilayers offer a wide variety of fascinating scientific effects and many applications in the magnetic recording industry.[1–3] An important class of magnetic multilayers contains antiferromagnetic (AFM) thin films. Such structures are used in the ultrasensitive magnetic read heads of today's advanced hard disk drives[4] and are likely to be used in tomorrow's nonvolatile magnetic memory devices.[5] In these structures the AFM layer is used to align (''pin'') a ferromagnetic reference layer thereby defining a preferred magnetic direction. Relative to this direction the magnetization of a second ferromagnetic layer can be switched. This results in a change of the electric resistivity of the structure, the giant magnetoresistance effect,[6] which can be exploited for reading or storing of information.

The pinning of the magnetization direction of a ferromagnetic layer by an adjacent AFM layer, so-called exchange bias, was discovered almost 50 years ago.[7] Despite active research on this topic, the exchange-bias effect is still poorly understood.[8,9] Clearly, the fundamental question is how the spin structure in the antiferromagnet influences that of the ferromagnet. Experimentally, the major obstacle with conventional tools has been the lack of sensitivity to the interface region. Neutron and optical techniques are bulk sensitive, and fail to give the required interface specific spin structure information. Also, in practice, the AFM films are quite thin (of the order of 50 nm) and the determination of the AFM structure in such thin films remains a challenge. For lack of better knowledge, models of exchange bias have therefore assumed that the AFM structure in thin films is identical to that in bulk single crystals and that the AFM structure at the ferromagnetic interface remains bulk like. Here we show that these assumptions can be incorrect.

Our study highlights the power of x-ray magnetic linear dichroism (XMLD) spectroscopy, carried out by means of surface-sensitive electron yield detection, for the determination of the AFM spin alignment in thin films and at surfaces. In particular, we report polarization-dependent soft x-ray absorption studies on structurally well-characterized AFM $LaFeO_3$ thin films, epitaxially grown on $SrTiO_3$ with different crystallographic orientations. We show that in all cases the magnetic structure in the near-surface layer of the epitaxial thin films differs significantly from that in the bulk. This is explained in terms of the close link between crystallographic strain and AFM order and domain structure. Our results point to the importance of using the true AFM structure near interfaces as the basis of realistic exchange coupling models.

II. EXPERIMENTAL DETAILS

The crystal structure of $LaFeO_3$ is sketched in Fig. 1(A). The parameters of the orthorhombic lattice, which belongs to the $Pbnm$ space group, are $a=5.557$ Å, $b=5.565$ Å, and $c=7.854$ Å.[10,11] $LaFeO_3$ is AFM with a bulk Néel temperature of 740 °C,[12] and the AFM axis is oriented along the crystallographic **a** axis.[13]

We studied thin $LaFeO_3$ films grown epitaxially on $SrTiO_3$ substrates with (110) and (100) surface orientations. The measurements presented here were obtained on 26 nm thin films, but we also investigated films with thicknesses ranging from 4 nm to 40 nm without finding any thickness dependence of our results. The films were prepared in a molecular beam epitaxy (MBE) system with film growth by means of a block-by-block method at 750 °C under a beam of atomic oxygen with a partial oxygen pressure of 5×10^{-6} Torr.[14] This method has been shown to yield high-quality epitaxial films.[15]

$SrTiO_3$ is an ideal substrate for epitaxial growth of $LaFeO_3$ because of its well-matching lattice constant of $a=3.905$ Å.[16] The gray planes in Fig. 1(A) indicate how the cubic (010) and $(\bar{1}10)$ planes of $SrTiO_3$ fit into the ortho-

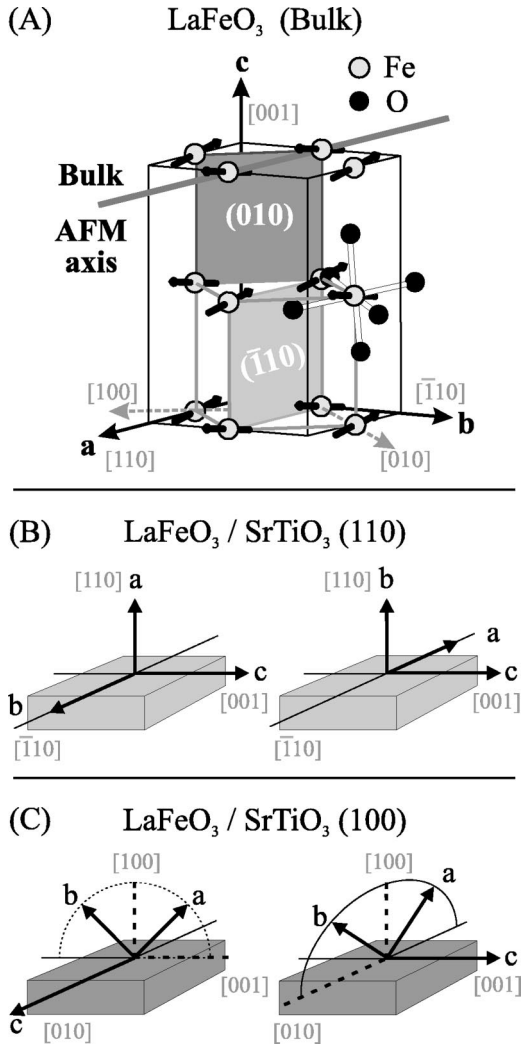

FIG. 1. (A) Orthorhombic unit cell of $LaFeO_3$. The AFM axis is oriented along the crystallographic **a** axis. The cubic notation refers to the quasicubic sublattice, which has lattice parameters close to those of cubic $SrTiO_3$. In (B) and (C), respectively, are sketched the crystallographic orientations of the twin domains in a $LaFeO_3$ film grown epitaxially on a $SrTiO_3$ (110) and (100) substrate. Note that the **c** axis lies in the film surface of all twinned domains.

rhombic $LaFeO_3$ lattice. The $LaFeO_3$ and $SrTiO_3$ lattice directions are indicated in the figure by the black and gray arrows and lines, respectively.

X-ray diffraction, plan view electron diffraction and conventional transmission electron microscopy (TEM) analysis[17,18] show that all epitaxial films consist of twinned crystallographic $LaFeO_3$ domains. Figure 1(B) illustrates the crystallographic orientations of the twinned $LaFeO_3$ domains in the case of the $SrTiO_3$ (110) substrate. Both twins grow with the $LaFeO_3$ **c** axis lying in the film surface oriented along the [001] axis of the $SrTiO_3$ (110) substrate, but they differ with respect to their **a**- and **b**-axis orientations. In one twin the **a** axis is out of plane, along [110], and the **b** axis lies in-plane along [1$\bar{1}$0]. In the other twin the **b** axis is out of plane and the **a** axis lies in the film plane.

The relative crystallographic orientation of the $SrTiO_3$ (110) substrate and the $LaFeO_3$ film is illustrated in Fig. 1(A) by the light gray area for the twin with the **a** and **c** axes lying in the film surface. This area indicates within the $LaFeO_3$ lattice the $SrTiO_3$ ($1\bar{1}0$) substrate surface, hence, the orientation of the $LaFeO_3$ lattice relative to the cubic axes of the $SrTiO_3$ substrate. The corresponding growth plane for the other twin is the $SrTiO_3$ (110) plane, which is obtained by rotating the $SrTiO_3$ ($1\bar{1}0$) plane by 90° around the [001] axis. The in-plane orientation along $SrTiO_3$ [001] of the **c** axis of these twinned domains gives the film macroscopically a twofold crystalline symmetry about the surface normal.

The crystallography of the twinned domains present in a $LaFeO_3$ film grown on a $SrTiO_3$ (100) substrate is illustrated in Fig. 1(C). Both twins have the **a** and **b** axes canted 45° from the film surface and the **c** axis lies in the film surface. The twins differ by their in-plane orientations of the **c** axis, which is oriented either along $SrTiO_3$ [010] or [001]. This gives the film a macroscopic fourfold crystalline symmetry about the surface normal.

Soft x-ray absorption experiments were carried out at the wiggler beamline 10-1 of the Stanford Synchrotron Radiation Laboratory (SSRL), which is equipped with a spherical grating monochromator. The energy scale of the monochromator was calibrated using the literature value of 706.8 eV for the L_3 absorption resonance of iron metal.[19] With the entrance and exit slit height set to 15 μm, the photon energy resolution is about 200 meV in the energy region around the Fe $L_{2,3}$ absorption edges. This enables us to resolve the Fe $L_{2,3}$ near-edge x-ray absorption fine structure (NEXAFS) of $LaFeO_3$ with negligible experimental broadening. The footprint of the beam on the sample was about 0.5 mm vertically and 1 mm horizontally and the spectra therefore represent averages over the micrometer-sized twin domains.

The photon beam of the wiggler beamline 10-1 is nearly linearly polarized. For photon energies close to the Fe $L_{2,3}$ absorption edges, 85% of the radiation intensity ($\propto|E^2|$) is linearly polarized in the horizontal plane, with the remaining 15% linearly polarized in the vertical plane. Experimental spectra can therefore be modeled as a linear superposition of two weighted spectra with orthogonal orientations of the **E** vector.[20] The two orthogonal polarization components are indicated by the axes of their electric field vectors $\mathbf{E}_h$ and $\mathbf{E}_v$ in Fig. 2. While the electric field vector components of the incident photon beam are fixed in space for our measurements, the sample can be rotated independently about various axes as shown in Fig. 2. In order to describe the orientation of the incident x rays relative to the sample we introduce a Cartesian coordinate system with the **z** axis parallel to the surface normal. In case of the $LaFeO_3$ film grown on a $SrTiO_3$ (100) substrate the two in-plane directions indicated by **x** and **y** are oriented parallel to the $SrTiO_3$ [010] and [001] axes, respectively, while they are oriented parallel to the $SrTiO_3$ [1$\bar{1}$0] and [001] axes, respectively, in the case of the $SrTiO_3$ (110) substrate. A rotation by an angle Θ about a vertical axis allows variation of the $\mathbf{E}_h$ component within the **x-z** plane (left panel) and, after a 90° sample rotation around the **z** axis, within the **y-z** plane (right panel). One notices that for these

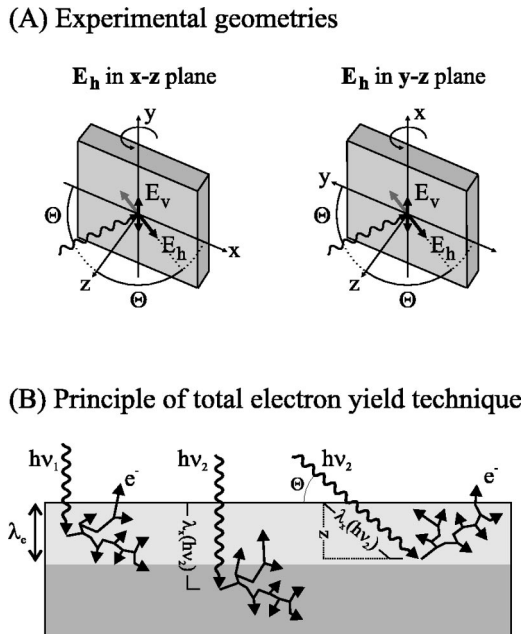

FIG. 2. (A) Sketch of the experimental geometry illustrating the orientation of the major horizontal $\mathbf{E}_h$ and minor vertical $\mathbf{E}_v$ linear polarized components of the elliptically polarized x rays. The x rays are incident on the sample under the angle Θ measured relative to the sample surface. The sample can be rotated independently about three orthogonal axes. When rotating the sample about a vertical axis, the major horizontal component $\mathbf{E}_h$ of the electric field vector rotates within the **x**-**z** (left) and **y**-**z** planes (right), respectively, with the angle between the $\mathbf{E}_h$ vector and the surface normal matching the photon incidence angle Θ. Independent of Θ, the minor vertical component $\mathbf{E}_v$ lies within the film surface oriented parallel to the **y** or **x** directions, respectively. The in-plane orientation of the major electric field vector component is changed by rotating the sample about the surface normal. Finally, the photon incidence angle can also be altered by rotating the sample around a horizontal axis in the surface plane. (B) Sketch of the electron scattering cascade following the Auger decay of a core electron vacancy. The probability for a secondary electron to escape from the sample decreases with increasing absorption length $\lambda_x(h\nu)$. λ_e gives the $1/e$ sampling depth measured perpendicular to the film surface, i.e., the thickness of the subsurface region, which contributes 67% to the measured yield spectrum. Going from a normal to a grazing incidence geometry, the effective x-ray penetration length perpendicular to the material surface is reduced to $z=\lambda_x \sin(\Theta)$.

rotations the vertical component remains fixed within the film surface, oriented parallel to the **y** and **x** directions, respectively.

For the soft x rays employed in our study, the x-ray penetration length of most materials is only fractions of a micrometer since the absorption is strong, and consequently transmission experiments require ultrathin samples. Total electron yield detection[20] is therefore the technique of choice for measuring absorption spectra of concentrated samples. The total electron yield (TEY) signal consists predominantly of inelastically scattered Auger electrons[20] as illustrated in Fig. 2(B). The TEY sampling depth is typically quoted as the $1/e$ effective electron escape depth λ_e,[21] which for the Fe $L_{2,3}$ absorption edges in $LaFeO_3$ is about 20 Å (see below).

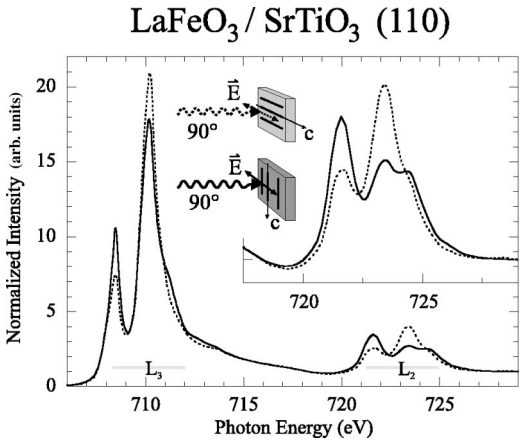

FIG. 3. Total electron yield (TEY) Fe $L_{2,3}$ NEXAFS spectra of $LaFeO_3$ [polarization-corrected (Ref. 23)] grown epitaxially on $SrTiO_3$ (110) as recorded for the two indicated normal incidence geometries using linearly polarized x rays. The two orthogonal orientations of the electric field vector relative to the $LaFeO_3$ **c** axis are obtained by rotating the sample around the surface normal relative to the incident x rays. The observed polarization dependence is referred to as x-ray magnetic linear dichroism (XMLD).

Our conclusions about the magnetic spin structure derived from the TEY absorption spectra therefore refer to the near-surface region of the film only. As discussed below, the TEY signal, after correction of saturation effects, is proportional to the x-ray absorption coefficient.

In the experiments discussed here, the TEY signal was obtained by measuring the sample photocurrent with a picoampère meter. The observed yield signal was normalized to the intensity of the incident photon beam as measured by the photocurrent of an 80% transmissive gold mesh. By normalizing all yield spectra to a common edge jump[22] well above the Fe L edges in the region 790–810 eV, the plotted spectra correspond to an absorption intensity per Fe atom.[20] As indicated in the figure captions, most spectra have in addition been corrected for the incomplete experimental x-ray polarization (thus corresponding to 100% linear polarization[20]) and saturation effects related to the TEY detection technique as discussed below.

III. RESULTS AND DISCUSSION

A. X-ray magnetic linear dichroism

Typical Fe $L_{2,3}$ NEXAFS spectra of $LaFeO_3$ are shown in Fig. 3. For both selected normal incidence geometries, the electric field vector of the linearly polarized x rays[23] lies in the surface plane of the $LaFeO_3$ film grown on $SrTiO_3$ (110). For the solid line spectrum the electric field vector is oriented perpendicular to the crystallographic **c** axis of both crystallographic twin domains present in the film, while it is oriented parallel to the **c** axis for the dashed line spectrum. The principal structure of the spectra is the same with two main peaks at both the L_3 and the L_2 absorption edges. Their comparison, however, reveals a pronounced polarization dependence with a similar signature at the L_3 and the L_2 edges. At both edges the first peak is higher for the **E** vector ori-

ented perpendicular to the **c** axis of the $LaFeO_3$ film, while for the **E** vector oriented parallel to the **c** axis the second peak is higher.

Since the six oxygen atoms surrounding each Fe atom in the $LaFeO_3$ crystal structure have a higher electronegativity than Fe, $LaFeO_3$ is an ionic compound in which Fe has a valency of 3+ and a d^5 high-spin ground state.[24] Correspondingly, the rich fine structure of the spectra can be explained by a multiplet calculation performed for an Fe^{3+} ion in a high-spin ground state,[24] which considers the multiplet coupling of the five Fe $3d$ valence electrons (or holes) in the ground state and the multiplet coupling of the four $3d$ holes and the $2p$ core hole in the final state. The oxygen ligands surrounding the Fe^{3+} ion give rise to an octahedral crystal field, which is taken into account via the cubic $10Dq$ crystal field parameter.

The spectra for $LaFeO_3$ can be interpreted in terms of the calculated spectra for α-Fe_2O_3.[25] In both materials the Fe atoms are surrounded by six oxygen atoms with the same local octahedral symmetry. Indeed, the x-ray absorption spectra of α-Fe_2O_3 and $LaFeO_3$ are nearly identical. Kuiper *et al.*[25] have determined the parameter $10Dq = 1.45$ eV for α-Fe_2O_3 and a value of 1.8 eV has been found for $LaFeO_3$ by Abbate *et al.*[24] Therefore, the same multiplet states contribute to the individual resonances of the two materials and the polarization dependence of the spectra has the same origin. In particular, Kuiper *et al.* showed experimentally and theoretically for α-Fe_2O_3 (Ref. 25) that the second peak of the L_3 and of the L_2 edge, i.e., the peaks at about 710 eV and 723.5 eV (see Fig. 3), are a particular convenient indicator for the orientation of the AFM axis relative to the x-ray electric field vector. Both peaks are largest when the **E** vector is parallel to the AFM axis and we shall use this result below.

In general, more than one multiplet state contributes to each of the peaks in the absorption spectrum.[26] Since these different states typically differ in their polarization dependence, the intensities of the absorption structures typically vary between two finite extreme values and do not vanish completely for any orientation of the electric field vector relative to the AFM axis. Therefore, at this point, we can only make a qualitative statement regarding the angular dependence in Fig. 3, namely, that for the geometry of the dashed spectrum the electric field vector is more closely aligned with the AFM axis than for the geometry of the solid spectrum. Hence, the averaged azimuthal orientation of the AFM axes of all domains contributing to the absorption spectrum is closest to the **c** axis.

This observation taken by itself is an important result, because without any analysis or manipulation of the experimental data, the linear dichroism revealed by these two ''as-measured'' spectra already indicates that the AFM structure in the near-surface layer of the thin epitaxially grown $LaFeO_3$ film is different from that in bulk $LaFeO_3$. To understand this conclusion, let us assume that within each of the twinned domains the AFM axis was oriented as in the $LaFeO_3$ bulk, i.e., along the crystallographic **a** axis. With reference to Fig. 1(B) we see that for a bulk like AFM axis orientation we should have a larger second peak for the **E** vector oriented perpendicular to the **c** axis, which is in contradiction to our observation. The orientation of the AFM axis can be determined quantitatively from a detailed analysis of the polarization dependence of the NEXAFS as discussed below.

B. Magnetic versus crystallographic x-ray linear dichroism

In nonmagnetic systems, the observation of an x-ray linear dichroism, i.e., the dependence of the absorption coefficient for linearly polarized x rays on the relative orientation of the sample and the axis of the electric field vector, indicates the presence of a charge asymmetry resulting from a bonding environment with lower than cubic symmetry. The best known examples are oriented molecules or polymer chains.[20,27] In magnetic systems, a polarization dependence can be induced by uniaxial magnetic order even in a cubic environment, a well-known example being NiO.[28,29] Even though the total charge in the atomic volume may remain isotropic, a polarization dependence relative to the magnetic axis can exist in resonances that correspond to transitions between specific multiplet states. This can give rise to strong x-ray magnetic linear dichroism (XMLD),[25,28,30] of interest here, where large intensity changes are observed when the electric field vector is aligned parallel and perpendicular to the magnetic axis.

Since only the local nearest-neighbor structure of Fe is cubic withinin the orthorhombic $LaFeO_3$ lattice, we need to first clarify that the observed polarization dependence does not arise from a crystallographic or bonding effect.[31,32] In cases where there is no structural transition any crystallographic polarization dependence should be unaffected by temperature. In contrast, a magnetic origin would be revealed by a disappearing dichroism as the Néel temperature is approached. In a previous publication[18] we have shown that for $LaFeO_3$ the magnitude of the polarization dependence decreases with temperature as expected from a purely magnetic origin. Due to sample degradation of $LaFeO_3$ at high temperatures in vacuum, however, we were unable to heat the thin film above its Néel temperature to fully quench the polarization dependence.

This temperature range limitation can be overcome by doping $LaFeO_3$ with strontium. From bulk studies it is known that the Néel temperature decreases with increasing Sr concentration.[11,33] For about 40% of the La atoms replaced by Sr, the Néel temperature drops below room temperature. We have grown a 40 nm thin $La_{0.4}Sr_{0.6}FeO_3$ film on a $SrTiO_3(110)$ substrate, for which the Néel temperature is expected to be around 200 K.[33] The Fe $L_{2,3}$ NEXAFS spectra of such a sample recorded below and above the Néel temperature are plotted in Figs. 4(A) and 4(B), respectively. We show polarization-dependent spectra recorded in the same experimental geometries as the $LaFeO_3$ spectra in Fig. 3. The spectra recorded at 100 K, well below the expected Néel temperature, reveal the presence of a strong polarization dependence, which completely vanishes in case of the room temperature spectra. This clearly demonstrates the purely magnetic origin of the linear dichroism observed for

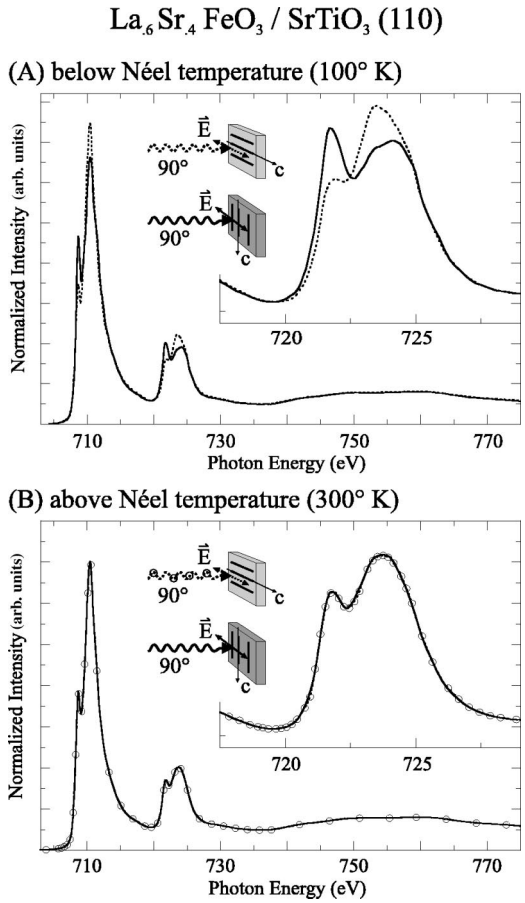

FIG. 4. Fe $L_{2,3}$ NEXAFS spectra [polarization-corrected (Ref. 23)] of $La_{0.6}Sr_{0.4}FeO_3$ for the two indicated geometries, (A) below and (B) above the Néel temperature. The absence of any dichroism above the Néel temperature demonstrates the magnetic origin of the dichroism observed below the Néel temperature. The origin of the broader absorption structures in comparison with $LaFeO_3$ is discussed in the literature (Ref. 24).

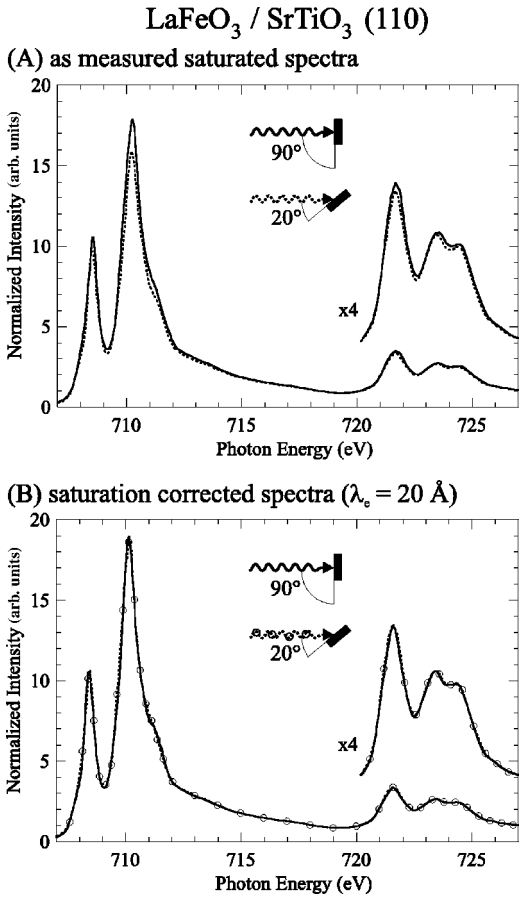

FIG. 5. (A) Normalized total electron yield spectra of $LaFeO_3$/$SrTiO_3$ (110) measured with the same in-plane orientation of the electric field vector in normal (black) and grazing (dashed) incidence geometry [polarization corrected (Ref. 23)]. The differences in peak heights and spectral shapes are due to saturation effects in the electron yield measurements. (B) The same spectra as in (A) corrected for saturation effects as discussed in the text using $\lambda_e = 20$ Å.

$La_{0.4}Sr_{0.6}FeO_3$ and $LaFeO_3$ below their respective Néel temperatures. We note that the overall spectral shape of the $La_{0.4}Sr_{0.6}FeO_3$ spectra is in agreement with the literature[24] and the observed polarization dependence is similar to that of the undoped $LaFeO_3$ film grown on $SrTiO_3$ (110). In particular, one notices that the orientation of the dichroism is the same for $La_{0.4}Sr_{0.6}FeO_3$ and $LaFeO_3$.

Our results are in good accord with previous findings that in transition metal oxides the spectral shape is mainly determined by the d^n electron ground state configuration and the local bonding symmetry.[34] As illustrated in Fig. 1(A), the six O atoms surrounding each Fe atom give a local octahedral symmetry with a single Fe-O distance of 1.963(1) Å in $La_{0.4}Sr_{0.6}FeO_3$ bulk and three nearly identical distances in $LaFeO_3$ bulk of 2.002(1) Å, 2.009(1) Å, and 2.010(1) Å. The noncubic symmetry of the $LaFeO_3$ lattice arises from the next-nearest-neighbor arrangement outside the octahedral Fe-O units within the crystal unit cell. We therefore conclude that the linear dichroism is of magnetic and not crystallographic origin.

C. Origin and correction of electron yield saturation effects

Quantitative determination of the direction of the AFM axis from the observed NEXAFS intensity variations requires that in addition to the elliptical polarization of the x rays a second experimental artifact is taken into account. This is the so-called saturation effect in yield measurements,[20] which has been carefully investigated for the $L_{2,3}$ absorption edges of the transition metals Fe, Co, and Ni (Refs. 35–39) and the iron oxides α-Fe_2O_3 and Fe_3O_4 (Ref. 40). In these yield spectra the height of the L_3 absorption resonances (the so-called white lines) is found to be reduced significantly.

The significance of saturation effects for $LaFeO_3$ is demonstrated in Fig. 5(A) showing two normalized TEY spectra,[22,23] which were recorded for the same in-plane orientation of the electric field vector, but at different incidence angles of the x rays relative to the film surface. The solid line spectrum was recorded at normal (90°) and the dashed spectrum at grazing incidence (20°). Although the overall shape of the two spectra is similar, the peak heights are significantly reduced in the grazing incidence spectrum.

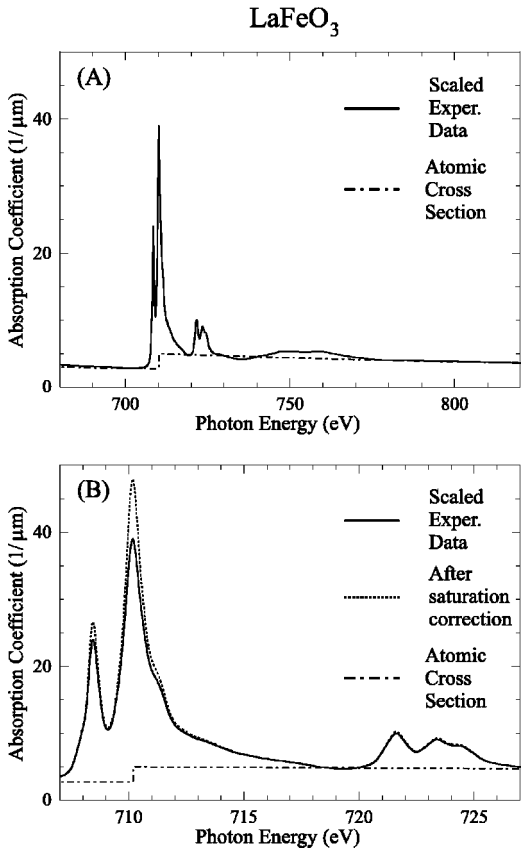

FIG. 6. (A) Scaling of a yield spectrum (solid line) outside of the resonance region to the calculated absolute atomic absorption coefficient (Ref. 43, dashed-dotted line) shown for the example of the $\Theta = 20°$ TEY spectrum from Fig. 5 (A). (B) Enlarged $L_{2,3}$ region of (A) showing in addition the saturation corrected spectrum (dotted line).

The origin of saturation effects in TEY measurements can be understood from Fig. 2(B). The x-ray absorption length is given by $\lambda_x(h\nu) = 1/\mu_x(h\nu)$, where $\mu_x(h\nu)$ is the x-ray linear absorption coefficient. Saturation effects become important when projection of the x-ray absorption length along the surface normal, $\lambda_x(h\nu)\sin(\Theta)$, becomes comparable to the effective electron escape depth λ_e, which is of the order of a few nanometers. This is most likely the case at resonance energies, where the absorption is strong, corresponding to a short absorption length, and also at grazing x-ray incidence, where $\sin(\Theta) \ll 1$ and the effective x-ray penetration is reduced by geometry.

As discussed in the literature, if the TEY sample composition is known, saturation effects in yield spectra can be corrected under certain conditions.[35,36,39,40–42] To do so one exploits the fact that saturation effects are generally negligible for photon energies far off any absorption edge, and that the absorption coefficient of a given element is nearly independent of the chemical environment in these energy regions. Scaling of the yield spectra to the calculated absorption coefficient in these regions [see Fig. 6(A)] transfers the arbitrary units of the yield spectrum to an absolute absorption coefficient scale (measured in units of length^{-1}). From these saturated data the unsaturated absorption coefficient can be calculated if the yield sampling depth is known.

As discussed in the literature[35,36,40] the sampling depth λ_e can be determined in specific experiments. In addition, we note that one may obtain λ_e from any two electron yield spectra, which have been recorded for the same **E**-vector orientation under different x-ray incidence angles Θ. The saturation-corrected absorption coefficients derived from such two experimental spectra will only match if the correct sampling depth is assumed. We have used this approach to derive λ_e for the two electron yield spectra shown in Fig. 5(A). With a value of $\lambda_e = 20$ Å for the TEY sampling depth of $LaFeO_3$ at the Fe $L_{2,3}$ edges we obtain the indistinguishable spectra plotted in Fig. 5(B). We note that this TEY sampling depth is surprisingly small, much closer to the value of 17 Å reported for metallic iron[35] than to the 50 Å and 35 Å reported recently for α-Fe_2O_3 and Fe_3O_4.[40] We speculate that the shorter sampling depth may result from the higher number of shallowly bound electrons of the lanthanum atoms replacing every other iron atom in the $LaFeO_3$ lattice.

This saturation-correction procedure yields automatically the saturation-corrected absolute absorption coefficient, which is plotted as a dotted line in Fig. 6(B). From the ordinate scale one can directly determine the x-ray absorption length $\lambda_x(710.2\ \text{eV}) = 208$ Å in $LaFeO_3$ for this particular **E** vector and AFM axis orientation. In particular, for an x-ray incidence angle of 20°, the effective x-ray penetration depth becomes only about 70 Å. Hence, $\lambda_x \approx 3\lambda_e$ only, and the saturation effects are expected to be significant, in line with the experimental observation shown in Fig. 5(A).

The saturation correction is limited in the case of the data discussed here by the experimental reproducibility of the spectra, because two, or in certain cases even three, different experimental spectra are necessary to calculate the spectra corresponding to pure linear polarization. Hence, any drift of the monochromator energy can affect peak heights and line shapes. The uncertainty of the saturation correction can be expressed as an uncertainty in the determined TEY sampling depth. We obtain $\lambda_e = 20 \pm 3$ Å.

Due to the short sampling depth only about the top 2 nm layer of the thin films contribute significantly to the spectra, and all conclusions drawn from the data apply only to this near-surface region. Within this region, however, we did not find any variation of the polarization dependence perpendicular to the film surface. To investigate any inhomogeneity over the sampled region, we recorded absorption spectra using Auger electron yield (AEY) detection.[20] The Fe *LVV* Auger electrons were detected by an electron energy analyzer in two geometries with the same electric field vector orientation but different electron take-off angles. For glancing electron take-off angles the AEY sampling depth is reduced to about one monolayer. We obtained identical AEY spectra, indicating that the spin structure was homogeneous, within experimental error, throughout the near-surface region.

D. XMLD spectra of $LaFeO_3/SrTiO_3$ (110)

The polarization-[44] and saturation-corrected XMLD spectra of $LaFeO_3/SrTiO_3$ (110) are plotted in Fig. 7 for the il-

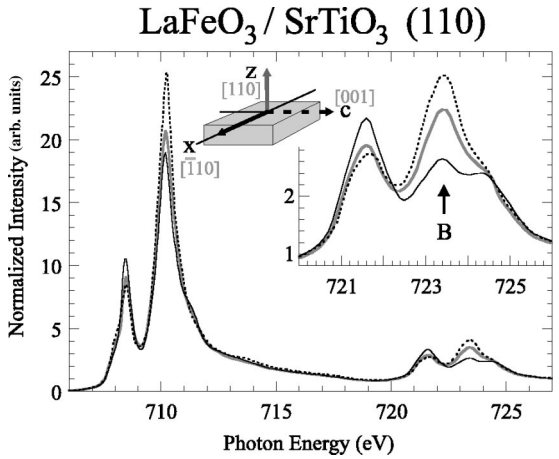

FIG. 7. Polarization- and saturation-corrected Fe $L_{2,3}$ NEXAFS spectra of $LaFeO_3/SrTiO_3$ (110) calculated from the experimental spectra for the indicated **E**-vector orientations. The electric field vector of the linearly polarized x rays is oriented perpendicular to the film (solid gray), in-plane parallel (dashed black), and perpendicular (solid black) to the **c** axes of both twinned crystallographic $LaFeO_3$ domains present in the film.

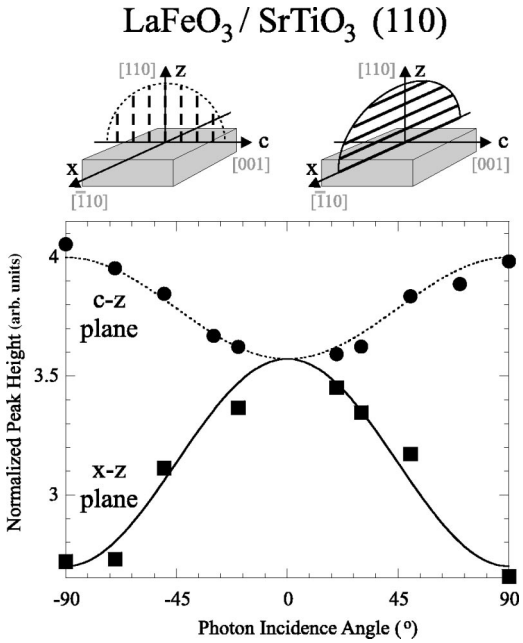

FIG. 8. Angular dependence of the (polarization- and saturation-corrected) intensity of peak *B* in Fig. 7 when rotating the electric field vector within the two indicated planes perpendicular to the film surface. Dots and squares refer to rotation of the **E** vector in the **c**-**z** and **x**-**z** plane (left and right figure in the upper panel), respectively. The photon incidence angle is given relative to the film surface, i.e., normal incidence corresponds to 90°, in which case the **E** vector is parallel to the film surface along the **c** axis (**x** direction) in the experimental geometry sketched in the left (right) part of the upper panel. The symmetrical shape of the data points relative to 0° incidence angle reflects the multidomain structure of the film. The black and gray lines are the result of a fit to the experimental data as discussed in the text.

lustrated orientations of the **E** vector along the three orthogonal sample axes. They were calculated from the measured spectra by use of the known linear polarization degree and the known $\cos^2(\Theta)$ angular dependence of the NEXAFS intensities (see below). For the dashed spectrum, the **E** vector is oriented along the **c** axis of both twinned crystallographic domains present in the film [see Fig. 1(B)]. For the other two **E**-vector orientations, along the **x** (solid black) and **z** directions (solid gray), an average of **a**-axis and **b**-axis orientations is measured because of the two twinned crystallographic domains.

Figure 7 shows clearly that all three spectra are different. These differences are not caused by saturation effect corrections, because for the L_2 edge saturation effects are only on the order of 3% (compare Fig. 5), while the observed dichroism for the peak labeled *B* exceeds 10% in all cases. The fact that the three spectra differ indicates that the AFM axis, averaged over the sampled domains, is not oriented parallel to any one of the three orthogonal axes shown in the figure.[45] If it were, two of the spectra in Fig. 7 would be identical. From analysis of the three spectra shown in Fig. 7 we see that the AFM axis is closest to the **c** axis.

In order to obtain a detailed picture of the AFM axis orientation we have measured spectra for the **E** vector located within two orthogonal planes that are both perpendicular to the film surface, as indicated in the top panel of Fig. 8. In the bottom panel we have summarized the polarization dependence by plotting the (polarization- and saturation-corrected) height of the second peak of the L_2 region (peak *B* in Fig. 7). Dots and squares indicate orientations of the electric field vector within the **c**-**z** and **x**-**z** planes, respectively. The two curves are symmetric relative to the surface normal (0° angle of incidence), reflecting the twofold magnetic symmetry of the sample.

From the observed angular dependence alone, it is not possible to quantitatively derive the direction of the AFM axis. The problem lies with insufficient knowledge about the peak heights for at least one of the extreme cases with the AFM axis parallel or perpendicular to the **E** vector. Since several multiplet states[24] contribute to each absorption structure, none of the peaks disappears for any geometry. In Sec. III I below we will show how this problem can be solved.

E. XMLD spectra of $LaFeO_3/SrTiO_3$ (100)

The saturation- and polarization-corrected NEXAFS spectra of $LaFeO_3/SrTiO_3$ (100) are plotted in Fig. 9. The solid and dashed lines correspond to the **E** vector oriented perpendicular and parallel to the film surface, respectively. The comparison of the two spectra reveals a dichroism effect, whose size is significant but considerably smaller than that observed for the film grown on the $SrTiO_3$ (110) surface.

When rotating the electric field vector within the film surface, one does not observe any in-plane dichroism. This indicates that the macroscopic orientation of the AFM axis has higher than twofold symmetry about the surface normal.[20] In fact, the absence of any in-plane dichroism is expected from the fourfold crystalline in-plane symmetry of the substrate and from the average over the two, each twofold symmetric,

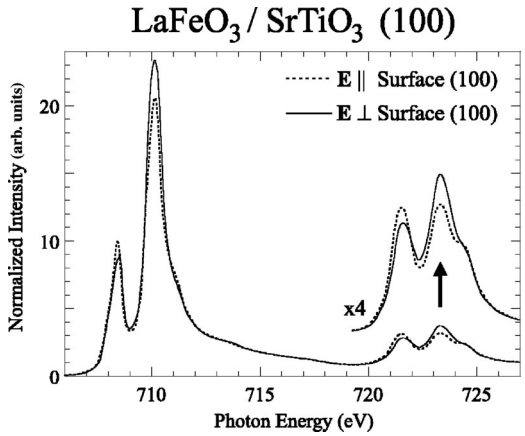

FIG. 9. Fe $L_{2,3}$ NEXAFS spectra (Ref. 23) of $LaFeO_3$ grown on a $SrTiO_3$ (100) substrate with the electric field vector in (dashed) and out of (solid) the surface plane [polarization (Ref. 23) and saturation corrected].

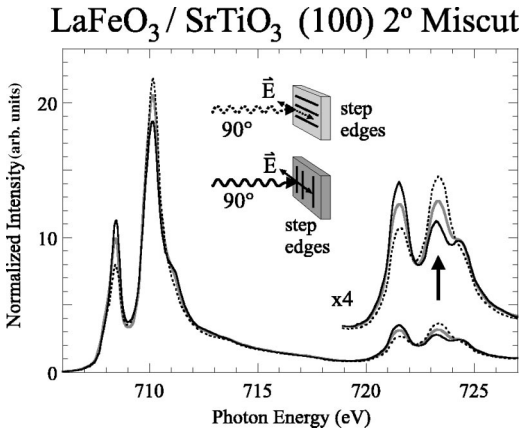

FIG. 10. Polarization-dependent Fe $L_{2,3}$ NEXAFS spectra of $LaFeO_3$ [polarization (Ref. 23) and saturation corrected] grown on a $SrTiO_3$ (100) substrate miscut by 2° along [001], giving a stepped surface with an average terrace width of 110 Å. TEM analysis shows that the in-plane anisotropy favors by 4:1 the growth of crystallographic $LaFeO_3$ domains with the **c** axis parallel to the step edges over twinned domains with the **c** axis perpendicular to the step edges. For the indicated geometries the electric field vector of the linearly polarized x rays is lying in the film surface oriented parallel (dashed black) and perpendicular (solid black) to the step edges. The gray line, which is in close agreement with the average of the other two spectra, is the spectrum recorded for the $LaFeO_3$ film grown on the flat $SrTiO_3$ (100) substrate with the electric field vector lying in the surface plane (taken from Fig. 9).

twin domains present in epitaxial $LaFeO_3$ on $SrTiO_3$ (100) as illustrated in Fig. 1(C). The angular dependence of the dichroism in the two spectra in Fig. 9 indicates that the AFM axis is tilted out of the surface plane.

F. XMLD spectra of stepped $LaFeO_3/SrTiO_3$ (100)

We also investigated a $LaFeO_3/SrTiO_3$ (100) sample grown on $SrTiO_3$ (100) that was miscut by 2° relative to the surface along [001]. This gives a (100) surface with approximately 110 Å wide terraces. X-ray diffraction (XRD) and TEM results for this sample reveal the same two twinned crystallographic domains present for $LaFeO_3$ grown on flat $SrTiO_3$ (100) [see Fig. 1(C)]. However, on the miscut substrate the growth of domains with the **c** axis oriented parallel to the step edges is favored by approximately 4:1 over those with the **c** axis perpendicular to the step edges.

The Fe $L_{2,3}$ XMLD spectra recorded for this film, shown in Fig. 10, reveal that the crystallographic in-plane asymmetry is accompanied by an in-plane magnetic asymmetry. The spectra correspond to an in-plane orientation of the **E** vector parallel (dashed black) and perpendicular (solid black) to the step edges. For comparison, we also show as a gray line the in-plane spectrum recorded for the $LaFeO_3$ film grown on the flat $SrTiO_3$ (100) substrate. This spectrum is identical to the average of the black and dashed spectra, within experimental accuracy. This is consistent with the intuitive expectation that the presence of steps just changes the relative abundance of the twin domains but that for a given twin domain the orientation of the AFM axis is identical for $LaFeO_3$ films grown on flat and stepped $SrTiO_3$ (100) substrates.

G. XMLD microscopy

Since the x-ray beam footprint on the sample is large compared to the size of the crystallographic domains, the spectroscopy results presented above give an average over the twin domains present in the film. Therefore the spectroscopy studies do not allow one to obtain reference spectra for the extreme situations of **E**-vector alignment parallel and perpendicular to the AFM axis. Such spectra are, however, essential for a quantitative determination of the AFM axis orientation in the films. In the following sections we show how this information can be obtained by spectromicroscopy,[46] i.e., spectroscopy with a lateral resolution smaller than the size of the twin domains.

For this purpose we used the photoemission electron microscope (PEEM) at the Advanced Light Source (ALS) in Berkeley.[47] Like the spectroscopy studies discussed above, PEEM measures the electron yield from the sample, except with additional lateral resolution. The resolution is provided by an electrostatic column that images electrons from a certain sample position onto a specific point on a phosphor screen that is read by a charge-coupled device camera. The image contrast in PEEM is due to variations in the local x-ray absorption coefficient, measured as changes in the local electron yield intensity. This gives PEEM all the properties of NEXAFS spectroscopy, namely, elemental specificity, chemical sensitivity, and magnetic sensitivity through x-ray magnetic circular (XMCD) and linear (XMLD) dichroism effects.

Figure 11 shows a PEEM image of a 40 nm $LaFeO_3$ film grown on a $SrTiO_3$ (100) bicrystal, which is made out of two $SrTiO_3$ (100) crystals joined together with their (110) and (010) faces. The resulting orientation of the crystallographic twin domains in the right and left halves of the bicrystal and the direction of **E** vector of the incident light are indicated in the inset. The photon energy selected to record this image matches the second peak of the L_2 absorption structure (see

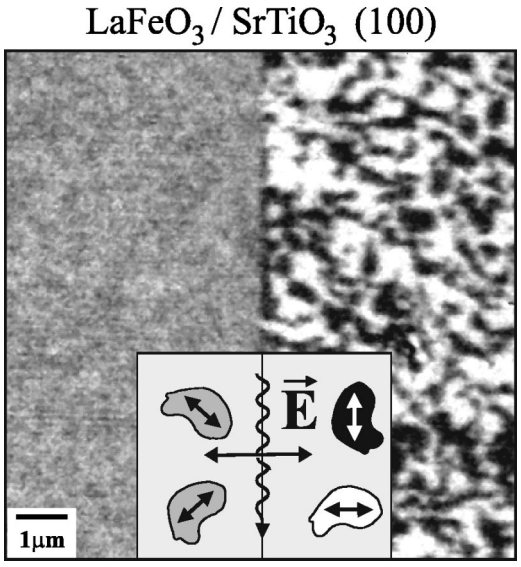

FIG. 11. Photoemission electron microscopy (PEEM) image of a $LaFeO_3$ film grown on a $SrTiO_3$ (100) bicrystal. The inset shows the direction of the **c** axes of the crystallographic domains in the two halves of the film and the direction of the electric field vector of the incident linearly polarized x rays. The photon energy used to record the image was 723.2 eV matching the second peak of the L_2 region (Ref. 48). The absence of any contrast on the left side is due to an equal 45° projection of the **E** vector onto the antiferromagnetic axes in the two twins. The image also suggests a correspondence of crystallographic and magnetic orientations.

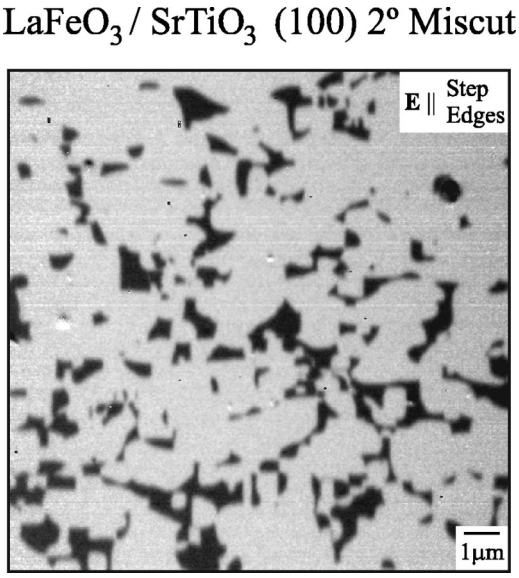

FIG. 12. PEEM image of a stepped $LaFeO_3$ film grown on $SrTiO_3$ (100) miscut by 2° along [001]. The image has been recorded with the electric field vector aligned parallel to the step edges and the selected photon energy of 723.2 eV matching the second peak of the Fe L_2 resonance (Ref. 48). Hence, bright (dark) regions correspond to antiferromagnetic domains with the in-plane projection of their antiferromagnetic axis parallel (perpendicular) to the electric field vector. The image shows that the area ratio of bright to dark regions follows the area ratio of crystallographic domains with the crystallographic axis parallel to perpendicular to the step edges. This suggests that the in-plane projection of the AFM axis is oriented parallel to the **c** axis.

arrow in Fig. 9).[48] Since the intensity of this peak is largest for the **E** vector parallel to the AFM axis, bright areas in the image reflect AFM domains with their AFM axis along **E**, black areas indicate domains with their AFM axis perpendicular to **E**, and gray areas indicate a 45° relative orientation. A careful study of the contrast dependence on azimuthal sample orientation showed that the maximum black/white contrast is obtained for parallel/perpendicular orientation of the **E** vector and the crystallographic **c** axes sketched in the right half of the figure inset, while for the 45° relative orientation sketched in the left half of the figure inset the domain contrast vanishes completely.

We conclude from the PEEM image and the observed angular dependence that the AFM domain structure of the $LaFeO_3/SrTiO_3$ (001) film has the same fourfold symmetry as the crystalline microstructure. They further show that the in-plane projection of the AFM axis is either parallel or perpendicular to the crystallographic **c** axis.

Figure 12 shows a PEEM image of the stepped $LaFeO_3$ film. The sample was oriented with the step edges parallel to the horizontal **E** vector of the linearly polarized x rays. The photon energy selected to record the image corresponds as before to the second peak of the L_2 absorption structure (see arrow in Fig. 10).[48] The image reveals clearly that the majority of the AFM domains has an in-plane projection of their AFM axes parallel to the step edges. Quantitative analysis yields the expected 4:1 ratio for the areas of domains appearing bright to dark in the image. The combined results of the two PEEM images therefore show that for $LaFeO_3$ on $SrTiO_3$ (100) within each domain the in-plane projection of the AFM axis is oriented along the crystallographic **c**-axis.

H. XMLD spectromicroscopy

By recording images as a function of photon energy, a so-called image stack, PEEM can be used for nanometer spectroscopy.[18,49,50] We have used the energy dependent image intensity of two different domains of a $LaFeO_3/SrTiO_3$ (100) sample (e.g., a bright and a dark domain of Fig. 11) to record single-domain x-ray absorption spectra. The local absorption spectra of the bright and dark domains are shown as open diamonds and solid circles in Fig. 13, respectively.

As discussed before, the bright and dark domains have a perpendicular in-plane projection of their respective AFM axes. Therefore we only know with certainty that for the dark domains the **E** vector is truly perpendicular to the AFM axis, independent of any out-of-plane orientation of the AFM axis. In the bright domains, however, the in-plane **E** vector is not parallel to the AFM axis, if this is oriented at an angle with the surface[51] (which we will show to be the case).

The lines in Fig. 13 reproduce the macroscopic NEXAFS spectra recorded on $LaFeO_3/SrTiO_3$ (110) with the **E** vector in the surface plane oriented parallel (dashed line) and perpendicular (solid line) to the **c** axis of the twinned domains (see Fig. 3). Comparison of the spectrum for the dark do-

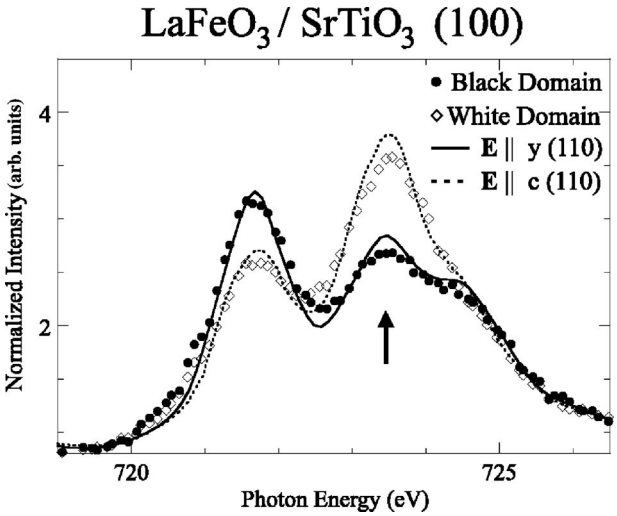

FIG. 13. Comparison of single-domain NEXAFS spectra (filled and open symbols) recorded by PEEM for $LaFeO_3/SrTiO_3$ (100) with macroscopically measured spectra of $LaFeO_3/SrTiO_3$ (110). The spectrum shown by the filled dots has been recorded in a dark region in Fig. 11 and closely resembles the macroscopically measured NEXAFS spectrum with the **E** vector oriented perpendicular to the **c** axis (solid line). The open symbols reproduce the spectrum recorded within a white region in Fig. 11. It is compared to the macroscopic spectrum recorded with the electric field vector parallel to the **c** axis. All four spectra are as measured with 85% of the radiation intensity linearly polarized in the horizontal plane.

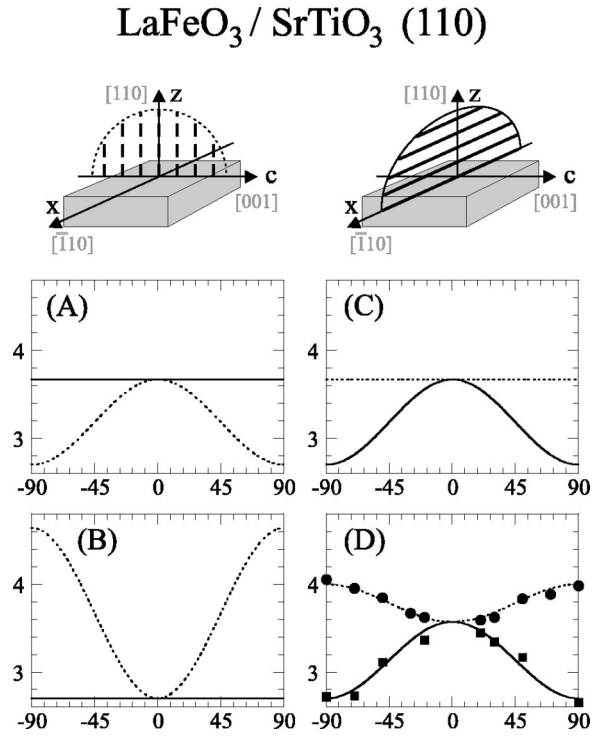

FIG. 14. Angular dependence of the intensity of peak *B* in Fig. 7 simulated for 100% linearly polarized x rays assuming the following orientation of the AFM axis within each microscopic domain (notation as in Fig. 8): (A) along the **a** axis as in bulk $LaFeO_3$; (B) along the **c** axis; (C) tilted 45° out-of-plane within the **c-z** plane; (D) tilted 35° out-of-plane within the **c-z** plane. Squares and circles in (D) are the experimental data reproduced from Fig. 8.

mains (black dots) with the solid line spectrum shows that they are very similar. After taking into consideration the diminished spectral resolution of the PEEM beam line [700 meV (Ref. 52)] relative to the SSRL spectroscopy beam line 10-1 (200 meV), we conclude that within experimental accuracy the two spectra are identical. The macroscopic XMLD spectrum given by the solid line must therefore correspond to an **E**-vector orientation perpendicular to the AFM axis of all domains in the $LaFeO_3/SrTiO_3$ (110) film. We therefore conclude that within each domain of the $LaFeO_3/SrTiO_3$ (110) film the AFM axis lies within the macroscopic **z-c** plane (see Fig. 7).

The local spectrum recorded within a bright domain of the $LaFeO_3/SrTiO_3$ (100) film (open diamonds) is also in close agreement with the macroscopically recorded NEXAFS spectrum with the electric field vector oriented along the **c** axis of the $LaFeO_3/SrTiO_3$ (110) film. This indicates very similar out-of-plane angles for the AFM axis in the two films [we find $\pm 35°$ for (110) versus $\pm 45°$ for (100) substrates; see below].

IV. ORIENTATION OF THE AFM AXIS IN $LaFeO_3$ FILMS

A. $LaFeO_3/SrTiO_3$ (110)

In order to quantitatively determine the AFM axis orientation in $LaFeO_3/SrTiO_3$ (110) we have simulated the angular dependence for various orientations of the AFM axis. For this simulation we included the information obtained from spectromicroscopy about the spectral shape for perpendicular orientation of **E** vector and AFM axis.[53] The contribution of each AFM domain *i* to the macroscopically averaging absorption spectrum is[28,54]

$$I(\alpha_i) = A + B\cos^2(\alpha_i), \tag{1}$$

where α_i is the angle between the AFM axis of domain *i* and the axis defined by the **E** vector of the incident linearly polarized photons. For a perpendicular orientation the contribution is given by the minimal intensity *A*, while the maximal intensity $A+B$ is obtained for a parallel orientation.

The angular dependence of the expected height of peak *B* in Fig. 7 for four different AFM axis orientations is plotted in Figs. 14(A)–14(D). We have assumed the same geometries as for the measured polarization dependence in Fig. 8 and the parameters are $A=2.70$ and $B=1.94$ (see below). In the case of Fig. 14(A) the bulk AFM axis orientation along the crystallographic **a** axis is assumed, which yields a polarization dependence in obvious disagreement with the experimental observation. Also in disagreement is the polarization dependence shown in Fig. 14(B), for which it is assumed that the AFM axis is oriented parallel to the **c** axis within each crystallographic domain. Figure 14(C) is obtained assuming that the AFM axis of each AFM domain lies within the **c-z** plane, tilted $\pm 45°$ out of the surface, independently of the crystal-

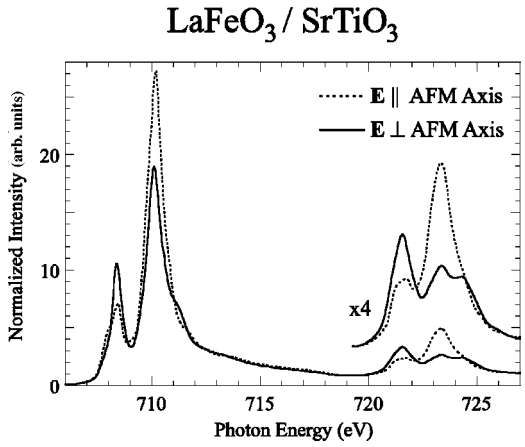

FIG. 15. Maximum amplitude of the XMLD effect of $LaFeO_3$ in the absence of saturation effects shown by the spectra corresponding to the electric field vector of 100% linearly polarized x rays oriented parallel (solid) and perpendicular (dashed) to the AFM axis. The parallel spectrum is calculated from the spectra shown in Fig. 7 using the determined orientation of the antiferromagnetic axis.

lographic orientation of the **a** and **b** axis. For this case the calculated angular dependence is closer to the experimental results in Fig. 8, which are reproduced by the dots and squares in Fig. 14(D). The major difference is that the experimental data indicate an angular dependence for both the **x-z** plane and the **c-z** plane. A simple change in the tilt angle of the AFM from $\pm 45°$ to $\pm 35°$ produces satisfactory agreement with the experiment, as shown in Fig. 14(D). A fit to the experimental data gives $A=2.70$, $B=1.94$ and a tilt angle of $\pm(35\pm 3°)$.

Having determined the direction of the AFM axis, we can calculate from the experimental data the spectrum that corresponds to the **E** vector aligned parallel to the AFM axis, which is experimentally not accessible in a macroscopic measurement due to the AFM domain structure of the film. This spectrum, shown by the dashed line in Fig. 15, is compared to the spectrum for the **E** vector aligned perpendicular to the AFM axis (solid line). The two spectra therefore represent the maximum XMLD effect for $LaFeO_3$, which for the L_2 edge gives an intensity change of about a factor of 2.

B. $LaFeO_3/SrTiO_3$ (100)

The tilt angle of the AFM axis in the case of the $LaFeO_3$ film grown on $SrTiO_3$ (100) can be determined by comparing the amplitude of the observed XMLD effect (Fig. 9) to the maximum XMLD effect (Fig. 15). Taking the fourfold symmetry of the AFM domain structure into account, one determines the AFM axis to be tilted by $\pm(45\pm 3)°$ out of the film surface. This is the same tilt angle as for the **a** and **b** axes of the twinned crystallographic domains [see Fig. 1(C)]. However, from the PEEM results we know that the AFM axis does not lie in the **a-b** plane, but is in the plane perpendicular to it, which contains the **c** axis. Hence, we find the AFM axis within the near-surface region of the $LaFeO_3$ film grown on $SrTiO_3$ (100) to be also rotated away from the bulk orientation towards the **c** axis.

The average of any three spectra measured for orthogonal orientations of the **E** vector is identical to the isotropic spectrum that one would measure on a polycrystalline sample.[55] Since the isotropic spectrum is solely determined by the chemical composition of a material, the isotropic spectra of $LaFeO_3$ films grown on $SrTiO_3$ (110) and (100) should be identical, which is indeed the case (comparison not shown). This comparison provides also a consistency check on the saturation- and polarization-correction procedures.

C. Stepped $LaFeO_3/SrTiO_3$ (100)

From Fig. 10 we concluded earlier that for a given twin domain the orientation of the AFM axis is identical for $LaFeO_3$ grown on flat and stepped $SrTiO_3$ (100) substrates. Hence, as for $LaFeO_3$ on flat $SrTiO_3$ (100) the tilt angle of the AFM axis should be $\pm 45°$. For the observed dichroism, this tilt angle corresponds to a ratio between AFM domains with the AFM axes parallel and perpendicular to the step edges of about 4:1. Since this is the same ratio as found by TEM and XRD for the twinned crystallographic domains, we conclude that the majority of the AFM domains has their AFM axis in the same direction as the majority of the microscopic crystallographic domains. This suggests that the AFM domain structure follows the crystallographic domain structure.

In the analysis of the observed dichroism either the tilt angle of the AFM axis or the ratio of the AFM domains is required as input. It is, however, equivalent, whatever information is known. Since the PEEM results shown in Sec. III G indicate that the ratio of the AFM domains is indeed close to 4:1, we can also interpret the spectroscopically observed dichroism as proof that microscopically the antiferromagnetism is not affected by the presence of the terraces.

D. Summary of results

Our results represent a detailed determination of the AFM spin structure in the near-surface region of a thin film. The orientations of the AFM axes for the investigated thin $LaFeO_3$ films are summarized in Fig. 16. The directions of the AFM axes for each of the twinned crystallographic domains are given by the dashed gray arrows. Black lines reproduce the crystallographic directions shown in Fig. 1(B) and 1(C). When the determined AFM orientations in the near-surface layer of the thin films are compared to that in the bulk [Fig. 1(A)] we find in all cases a significant deviation. In the thin film surfaces the AFM axis orientation appears to be largely determined by the direction of the **c** axis and the presence of the film surface, since in all cases the AFM axis points out of the film surface and its in-plane projection lies along the **c** axis.

The presence of steps favors the growth of those twinned crystallographic domains, which have their **c** axis parallel to the step edges. We find complete agreement between the ra-

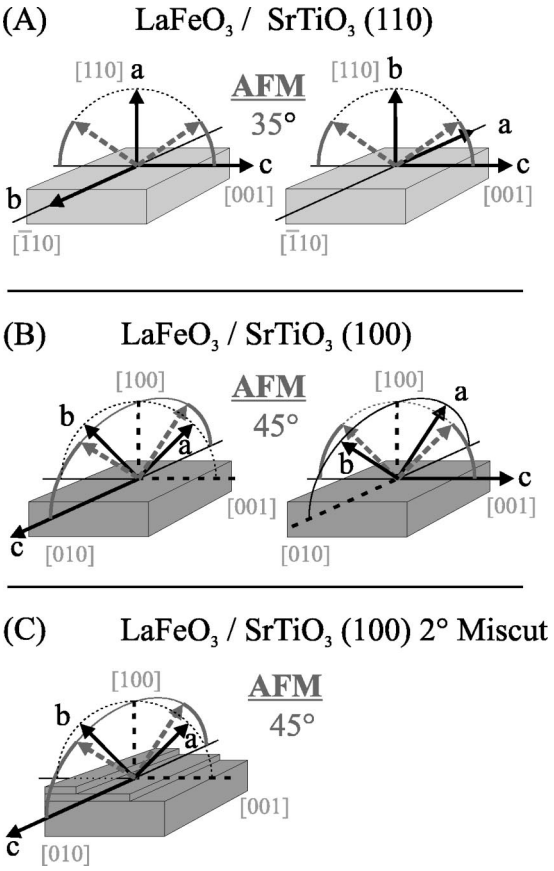

FIG. 16. Summary of the crystallographic (solid black) and AFM (dashed gray) orientations in the near-surface region of thin $LaFeO_3$ films epitaxially grown on three different $SrTiO_3$ substrates as indicated. In all cases the in-plane projection of the antiferromagnetic axis is oriented parallel to the crystallographic **c** axis. (C) shows the AFM axis of the majority twins of the two crystallographic domains.

tio of crystallographic twins and magnetic twins, indicating that the microscopic crystallographic structure dictates the microscopic AFM structure. AFM domain walls should therefore follow crystallographic domain boundaries. This is understandable because of the absence of dipolar fields in antiferromagnets. Hence, there is no energetic penalty due to dipolar fields for introducing a domain boundary at a crystallographic discontinuity. Consequently, it may be energetically favorable that the AFM axis is oriented within each microscopic domain along an easy AFM direction.

The tilt angles of the AFM axis to the film surface are $\pm 35°$ for $SrTiO_3$ (110) and $\pm 45°$ for $SrTiO_3$ (100) substrates. These angles correspond to the intersection angle of (111) planes with the film surfaces as illustrated in Fig. 17. The (111) planes are shown within the cubic lattice of the $SrTiO_3$ substrate, and the light gray areas give the orientation of the $LaFeO_3$ film surfaces. The orientations of the AFM axes are given by black lines. In all cases, these lines fall within a (111) plane, which are indicated in dark gray.

We conclude that for the investigated thin epitaxial $LaFeO_3$ films the orientation of the AFM axis in the near-surface region is determined by the direction of the in-plane

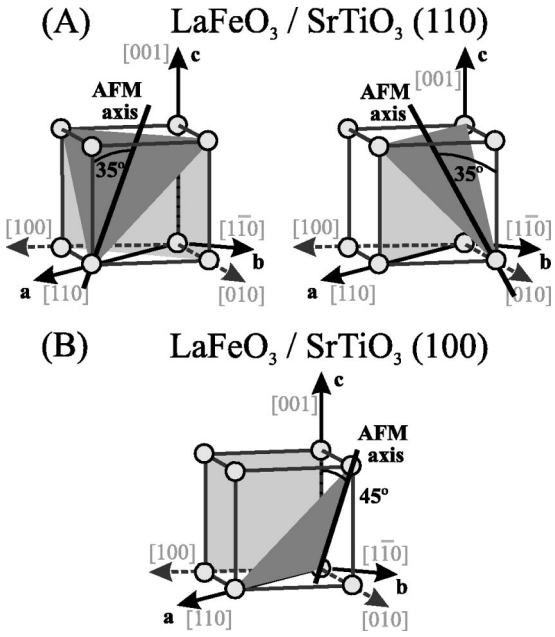

FIG. 17. Illustration showing that for the near-surface region of all studied thin films the AFM axis (black line) lies within a (111) plane (dark gray) of the quasicubic sublattice, with a projection onto the surface plane (light gray) that is along the **c** axis.

c axis and the condition to lie within a (111) plane of the quasicubic sublattice of $LaFeO_3$. Since within the *Pbnm* space group this orientation of the AFM axis is not permitted due to symmetry considerations, one has to conclude that the crystal symmetry in these thin films differs from that of bulk $LaFeO_3$. We note that a deviation of the AFM axis from the ideal bulk direction, and therefore a change in crystal symmetry, has also been observed for polycrystalline $LaFeO_3$.[56]

As mentioned before, we have found identical polarization dependencies for films with thicknesses ranging from 4 nm to 40 nm. This suggests that for this thickness range the derived orientation of the AFM axis also applies to the ''bulk'' of the thin films, but a rigorous proof would require a bulk sensitive measurement.

V. CONCLUSIONS

We have shown that x-ray magnetic linear dichroism spectroscopy can be used to obtain detailed information on the AFM spin structure of surfaces. The AFM structure is found to differ markedly from the bulk case. This has important implications, e.g., for the understanding of exchange-bias phenomena. One of the crucial assumptions made in most of the current exchange-bias models is shown to be incorrect, namely, that the exchange coupling of a ferromagnet is determined by the bulk like AFM spin structure.

ACKNOWLEDGMENTS

The authors acknowledge E.E. Fullerton and M.F. Toney for fruitful discussions and their XRD analysis of the microcrystalline domain structure of the $LaFeO_3$ films, in particular, of the one grown on the miscut $SrTiO_3$ substrate. Fur-

thermore, the authors express their thanks to Jeff Moore and Curtis Troxel for their support at the Stanford Synchrotron Radiation Laboratory (SSRL) where the NEXAFS experiments have been carried out. SSRL is supported by the Department of Energy, Office of Basic Energy Science. Support by the Swiss National Science Foundation is acknowledged by F.N. and J.W.S. The spectromicroscopy experiments were performed at the PEEM2 microscope of the ALS, Berkeley, which is also supported by the Department of Energy, Office of Basic Energy Science.

---

*Present address: Swiss Light Source, Paul Scherrer Institute, CH-5232 Villigen–PSI, Switzerland.

†Present address: Institut de Physique de la Matière Complexe, Ecole Polytechnique Fédéral de Lausanne, CH-1015 Lausanne, Switzerland.

[1] P. Grünberg, Phys. Today **54**(5), 31 (2001).

[2] L. Thomas, J. Lüning, A. Scholl, F. Nolting, S. Anders, J. Stöhr, and S.S.P. Parkin, Phys. Rev. Lett. **84**, 3462 (2000).

[3] R.D. Hempstead, S. Krongelb, and D.A. Thompson, IEEE Trans. Magn. **14**, 521 (1978).

[4] A. Moser, C.T. Rettner, M.E. Best, E.E. Fullerton, D. Weller, M. Parker, and M.F. Doerner, IEEE Trans. Magn. **36**, 2137 (2000).

[5] S.S.P. Parkin, K.P. Roche, M.G. Samant, P.M. Rice, R.B. Beyers, R.E. Scheuerlein, E.J. O'Sullivan, S.L. Brown, J. Bucchigano, D.W. Abraham, Y. Lu, M. Rooks, P.L. Trouilloud, R.A. Wanner, and W.J. Gallagher, J. Appl. Phys. **85**, 5828 (1999).

[6] P. Grünberg, S. Demokritov, A. Fuss, M. Vohl, and J.A. Wolf, J. Appl. Phys. **69**, 4789 (1991).

[7] W.H. Meiklejohn and C.P. Bean, Phys. Rev. **102**, 1413 (1956).

[8] J. Nogués and I.K. Schuller, J. Magn. Magn. Mater. **207**, 7 (1999).

[9] A.E. Berkowitz and K. Takano, J. Magn. Magn. Mater. **200**, 552 (1999).

[10] H.F. McMurdie, M.C. Morris, E.H. Evans, B. Paretzkin, W. Wong-Ng, and C.R. Hubbard, Powder Diffr. **1**, 269 (1986); W.C. Koehler and E.O. Wollan, J. Phys. Chem. Solids **2**, 100 (1957).

[11] S.E. Dann, D.B. Currie, M.T. Weller, M.F. Thomas, and A.D. Al-Rawwas, J. Solid State Chem. **109**, 134 (1994).

[12] M. Eibschütz, S. Shtrikman, and D. Treves, Phys. Rev. **156**, 562 (1967); G.H. Jonker, Physica (Amsterdam) **22**, 707 (1956).

[13] R.L. White, J. Appl. Phys. **40**, 1061 (1969).

[14] J.-P. Locquet, A. Catana, E. Mächler, C. Gerber, and J.G. Bednorz, Appl. Phys. Lett. **64**, 372 (1994).

[15] J.-P. Locquet, J. Perret, J. Fompeyrine, E. Machler, J.W. Seo, and G. Van Tendeloo, Nature (London) **394**, 453 (1998).

[16] A.F. Wells, *Structural Inorganic Chemistry*, 4th ed. (Clarendon Press, Oxford, 1975).

[17] J.W. Seo, J. Fompeyrine, H. Siegwart, and J.-P. Locquet, in *Transport and Microstructural Phenomena in Oxide Electronics*, edited by D.S. Ginley, D.C. Paine, M.E. Hawley, S.K. Streiffer, and D.H.A. Blank, MRS Proc. No. 666 (Materials Research Society, Warrendale, PA, 2001).

[18] A. Scholl, J. Stöhr, J. Lüning, J.W. Seo, J. Fompeyrine, H. Siegwart, J.-P. Locquet, F. Nolting, S. Anders, E.E. Fullerton, M.R. Scheinfein, and H.A. Padmore, Science **287**, 1014 (2000).

[19] C.T. Chen, Y.U. Idzerda, H.-J. Lin, N.V. Smith, G. Meigs, E. Chaban, G.H. Ho, E. Pellegrin, and F. Sette, Phys. Rev. Lett. **75**, 152 (1995).

[20] J. Stöhr, *NEXAFS Spectroscopy*, Vol. 25 of Springer Series in Sciences (Springer, Heidelberg, 1992).

[21] Generally, the TEY sampling depth will depend on the photon energy as the contribution of primary photoelectrons varies with the photon energy. This is shown for the case of Au and Cu by H. Henneken, F. Scholze, and G. Ulm, J. Appl. Phys. **87**, 257 (2000). Over a small energy range as in the spectra discussed here, however, the TEY sampling depth is to a good approximation constant.

[22] Since the scale of yield spectra is generally arbitrary, it is convenient for the comparison of spectra from different samples to set the yield spectrum before the absorption edge to zero and to adjust the slope of the spectrum such that it is constant in a region far above the absorption resonance. Hence, the normalized spectra show the intensity of the edge of interest per absorbing atom (Ref. 20).

[23] The spectra shown have been corrected for finite polarization degree of the x rays and correspond to 100% (horizontal) linear polarization.

[24] M. Abbate, F.M.F. de Groot, J.C. Fuggle, A. Fujimori, O. Strebel, F. Lopez, M. Domke, G. Kaindl, G.A. Sawatzky, M. Takano, Y. Takeda, H. Eisaki, and S. Uchida, Phys. Rev. B **46**, 4511 (1992).

[25] P. Kuiper, B.G. Searle, P. Rudolf, L.H. Tjeng, and C.T. Chen, Phys. Rev. Lett. **70**, 1549 (1993).

[26] F.M.F. de Groot, J.C. Fuggle, B.T. Thole, and G.A. Sawatzky, Phys. Rev. B **42**, 5459 (1990).

[27] J. Stöhr and M.G. Samant, J. Electron Spectrosc. Relat. Phenom. **98**, 189 (1999).

[28] D. Alders, L.H. Tjeng, F.C. Voogt, T. Hibma, G.A. Sawatzky, C.T. Chen, J. Vogel, M. Sacchi, and S. Iacobucci, Phys. Rev. B **57**, 11 623 (1998).

[29] H. Ohldag, A. Scholl, F. Nolting, S. Anders, F.U. Hillebrecht, and J. Stöhr, Phys. Rev. Lett. **86**, 2878 (2001).

[30] G. van der Laan, B.T. Thole, G.A. Sawatzky, J.B. Goedkoop, J.C. Fuggle, J.-M. Esteva, R. Karnatak, J.P. Remeika, and H.A. Dabkowska, Phys. Rev. B **34**, 6529 (1986).

[31] P. Carra, H. König, B.T. Thole, and M. Altarelli, Physica B **192**, 182 (1993).

[32] G. van der Laan, Phys. Rev. B **57**, 5250 (1998).

[33] U. Shimony and J.M. Knudsen, Phys. Rev. **144**, 361 (1966).

[34] F.M.F. de Groot, J. Electron Spectrosc. Relat. Phenom. **67**, 529 (1994); Chem. Rev. (Washington, D.C.) **101**, 1779 (2001).

[35] R. Nakajima, J. Stöhr, and Y.U. Idzerda, Phys. Rev. B **59**, 6421 (1999).

[36] V. Chakarian, Y.U. Idzerda, and C.T. Chen, Phys. Rev. B **57**, 5312 (1998).

[37] J. Hunter Dunn, D. Arvanitis, N. Mårtensson, M. Tischer, F. May, M. Russo, and K. Baberschke, J. Phys.: Condens. Matter **7**, 1111 (1995).

[38] J. Vogel and M. Sacchi, Phys. Rev. B **49**, 3230 (1994).

[39] W.L. O'Brien and B.P. Tonner, Phys. Rev. B **50**, 12 672 (1994).

[40] S. Gota, M. Gautier-Soyer, and M. Sacchi, Phys. Rev. B **62**, 4187 (2000).

[41] B.T. Thole, G. van der Laan, J.C. Fuggle, G.A. Sawatzky, R.C. Karnatak, and J.-M. Esteva, Phys. Rev. B **32**, 5107 (1985).

[42] T.J. Regan, H. Ohldag, C. Stamm, F. Nolting, J. Lüning, J. Stöhr, and R.L. White, Phys. Rev. B **64**, 214422 (2001).

[43] B.L. Henke, E.M. Gullikson, and J.C. Davis, At. Data Nucl. Data Tables **54**, 181 (1993). A convenient tabulation can be found at www-cxro.lbl.gov.

[44] Due to the in-plane asymmetry of the film, the spectrum corresponding to the electric field vector perpendicular to the film surface can be calculated outgoing from two different 20° grazing incidence spectra. This can be used as a check for consistency, since the resulting **E** perpendicular spectra have to be identical.

[45] Without making any assumption for the quantitative or even the qualitative relation between spectral intensity and the relative orientation of electric field vector and antiferromagnetic axis, one can therefore conclude that the antiferromagnetism of the thin $LaFeO_3$ film differs from the bulk case.

[46] J. Stöhr, H.A. Padmore, S. Anders, T. Stammler, and M.R. Scheinfein, Surf. Rev. Lett. **5**, 1297 (1998).

[47] S. Anders, H.A. Padmore, R.M. Duarte, T. Renner, T. Stammler, A. Scholl, M.R. Scheinfein, J. Stöhr, L. Seve, and B. Sinkovic, Rev. Sci. Instrum. **70**, 3973 (1999).

[48] The PEEM images shown are obtained by division of two images recorded for photon energies corresponding to opposite XMLD effects at the L_2 edge, i.e., the photon energy for the first image is indeed 723.3 eV, while for the second image a photon energy of 721.3 eV has been used. As discussed in detail elsewhere (Refs. 18 and 50) this only enhances the XMLD contrast.

[49] F. Nolting, A. Scholl, J. Stöhr, J.W. Seo, J. Fompeyrine, H. Siegwart, J.-P. Locquet, S. Anders, J. Lüning, E.E. Fullerton, M.F. Toney, M.R. Scheinfein, and H.A. Padmore, Nature (London) **405**, 767 (2000).

[50] A. Scholl, H. Ohldag, F. Nolting, J. Stöhr, and H.A. Padmore, Rev. Sci. Instrum. **73**, 1362 (2002).

[51] An alignment of the electric field vector parallel to the antiferromagnetic axis would then require to rotate the electric field vector out of the film surface, which is not possible in the current PEEM setup (Ref. 47).

[52] In addition to the limited resolution of only $E/dE \approx 1000$ a non-Gaussian photon energy distribution gives rise to significant broadening of the absorption structures in the local PEEM absorption spectra.

[53] Alternatively, one could use—if available—the information about the spectral shape for parallel alignment of the **E** vector and the antiferromagnetic axis.

[54] J. Stöhr, A. Scholl, T.J. Regan, S. Anders, J. Lüning, M.R. Scheinfein, H.A. Padmore, and R.L. White, Phys. Rev. Lett. **83**, 1862 (1999).

[55] J. Stöhr and M.G. Samant, J. Electron Spectrosc. Relat. Phenom. **98**, 189 (1999).

[56] T. Peterlin-Neumaier and E. Steichele, J. Magn. Magn. Mater. **59**, 351 (1986).